Journal of Environmental Chemical Engineering xxx (xxxx) 109553

Contents lists available at ScienceDirect

Journal of Environmental Chemical Engineering

journal homepage: www.elsevier.com/locate/jece

Photocatalytic degradation and pollutant-oriented structure-activity analysis of carbamazepine, ibuprofen and acetaminophen over faceted TiO_2

Szymon Dudziak, Agnieszka Fiszka Borzyszkowska, Anna Zielińska-Jurek *

Department of Process Engineering and Chemical Technology, Gdańsk University of Technology, G. Narutowicza street 11/12, 80-233 Gdańsk, Poland

ARTICLE INFO

Keywords:
Crystal facets
Pharmaceuticals degradation
Photocatalysis
Correlation model

ABSTRACT

Photocatalytic degradation of carbamazepine, ibuprofen, acetaminophen and phenol was studied in the presence of anatase photocatalyst, exposing three different crystal facets in the majority of {0 0 1}, {1 0 0} or {1 0 1}. It was found that octahedral anatase particles exposing {1 0 1} facets allow to achieve the best degradation and mineralization of all persistent organic pollutants. This confirms that the previous findings, showing high {1 0 1} activity, are not limited to phenol and could be generalized for other water pollutants. Based on the obtained results, a correlation model including exposed TiO_2 crystal facet and chemical hardness of the pollutant was developed to predict the degradation rate of pollutants with a possibly diverse electronic structure. The structure-activity analyses, based on the reactivity predictors obtained from the DFT calculations for all tested compounds, have shown that pollutants with higher chemical hardness react faster with the photocatalyst. Alternatively, a similar effect was observed for the higher HOMO-LUMO energy gap of the compound. This relation indicates that for compounds with a low energy position of LUMO orbital, e.g., carbamazepine, process efficiency is not strictly dependent on the stability of h^+ generated organic radical, which is often pointed out as an initial reactive form. Based on these results, a correlation model was developed for the first time to quantitatively describe the effect of the facet-pollutant interactions based on their independent electronic properties. Finally, this was followed by the detailed degradation study of the pharmaceuticals mixture, showing the impact of the total concentration and role of active species on the degradation efficiency over facet-engineered TiO_2 photocatalysts.

1. Introduction

A growing human population has led to a significant increase in the consumption of pharmaceuticals. Commonly used pharmaceutical compounds such as carbamazepine (CBZ), ibuprofen (IBU) and acetaminophen (ACT, also known as paracetamol) are currently detected in the aqueous environment worldwide [1,2]. The occurrence of some pharmaceuticals in surface waters presents a global challenge considering their potential for bioaccumulation and biomagnification. For example, the removal efficiency of carbamazepine from wastewater treatment plant effluents is about 10% due to low sorption properties on activated sludge microorganisms. Therefore, compounds like carbamazepine are not susceptible to biodegradation using conventional water treatment processes [2,3]. For carbamazepine, the environmental concentrations are close to the threshold value affecting plasma 11-ketotestosterone concentration in male fish, while for ibuprofen, it exceeded the threshold for decreasing fish egg fertilization (about 100 ng•dm^{-3} for IBU [3] and 500 ng•dm^{-3} for CBZ [4]). Bioaccumulation of both carbamazepine and ibuprofen is reported to easily occur in mussels, achieving 90 (CBZ) and 460-fold (IBU) concentration increase in the tissue [5]. Parolini et al. reported that even acetaminophen concentrations as low as 1.5 μg•dm^{-3} could induce a cyto-genotoxic effect on zebra mussels [6]. Furthermore, the study by Galus et al. has shown that chronic exposure to ACT and CBZ induces histopathological changes in zebrafish kidneys, as well as increases embryo mortality [4]. Finally, in the case of carbamazepine, toxic by-products, especially acridine, and acridone, can form during the photolysis process, which increases the toxicity of the aqueous phase [7,8]. In this regard, all these compounds are considered pharmaceutical active compounds (PhACs), belonging to the group of emerging pollutants of major concern. Therefore, there is a need to develop effective technologies that allow a more significant reduction of toxic PhACs, which are not susceptible to biodegradation, to solve the current water pollution problem.

Photocatalysis is one of the successful methods that remove persistent organic pollutants and is also classified as green technology. However, although a great effort was made in the field of photocatalytic wa-

* Corresponding author.
E-mail addresses: dudziakszy@gmail.com (S. Dudziak), annjurek@pg.edu.pl (A. Zielińska-Jurek).

https://doi.org/10.1016/j.jece.2023.109553
Received 22 December 2022; Received in revised form 8 February 2023; Accepted 18 February 2023
2213-3437/© 20XX

ter purification, including (i) photocatalyst composition [9–14], (ii) process optimization [15,16], and (iii) reactor design [17,18], there are still some challenges concerning detailed photocatalyst design for the particular application in photocatalytic process. This especially concerns the surface structure of the photocatalyst, which can be modified by the exposition of suitable crystal facets [19,20]. Furthermore, photocatalytic reactions are still difficult to describe precisely through model development due to the complexity of the involved reactions. More recently, computational simulations allowed to study elementary steps of these processes on a fundamental level, providing a general description of how the overall process could be initiated [21–23]. However, regarding photocatalytic water treatment from emerging contaminants, a relationship between observed process efficiency and the results obtained from the computational studies is generally not present in the literature so far. Recently, we have studied such an approach and observed that phenol and toluene degradation efficiency as model organic pollutants over the different anatase facets depend mostly on the probability of trapping electrons and holes on the surface atoms [24]. This probability is proportional to the reported "trapping energy" for these surface structures [25], which is the energy gain of the system when an electron or hole becomes localized on the surface atoms. Therefore, the degradation process over the TiO_2 photocatalyst is mostly controlled by the distribution of surface trapped states, specific for each crystal facet (highest density for the {1 0 1} facets and the lowest for {0 0 1} one). Following the previous findings for the phenol degradation, the observed per-second rate constant (k) can be described with the following Eq. (1) [24]:

$$k = A \cdot E_{surf} \cdot \left(\frac{n_{trap}}{n_{pollutant}}\right)^{1/2} \cdot \left(e^{\frac{B \cdot E_{trap}}{kT}} - 1\right) + k_0 \quad (1)$$

where A and B are fitted constants, E_{surf} is the surface energy of the dominant facet, n_{trap} is the number of the trapping centers on the surface of the photocatalyst (calculated from the photocatalyst's mass, BET surface area and atomic model of the dominant facet [25]), $n_{pollutant}$ is a number of pollutant molecules at the start of the process, E_{trap} is a sum of trapping energies reported for both holes and electrons for the dominant facet [25], kT is a product of Boltzman constant and temperature and k_0 is spontaneous photolysis of the pollutant. This specific relation showed a very good correlation with the degradation rate of phenol, however, due to a large number of possible contaminants, it seems necessary to further investigate the accuracy of the model with respect to the different water-phase pollutants.

In this regard, in the present study, TiO_2 photocatalysts exposing the majority of {0 0 1}, {1 0 0}, and {1 0 1} crystal facets were synthesized and systematically studied in the degradation of carbamazepine, ibuprofen, and acetaminophen. The novelty of the present work is focused on three aspects: (i) cross-investigation of the facet-pollutant interactions, based on the electronic properties of both of them; (ii) quantitative description of these interactions through the development of the statistical model and (iii) degradation experiments of the pharmaceuticals mixture, using facet-engineered photocatalysts. The combination of real-life water pollutants with TiO_2 exposing specific crystal facets allowed us, for the first time to show and discuss the photocatalytic activity concerning both photocatalyst surface structure and chemical structure of the pollutant. Furthermore, photocatalytic studies were completed with the phenol (PHE) degradation analyses as a relative comparison with previous works. Finally, degradation tests of the pharmaceuticals mixture using facet-engineered photocatalysts were also performed to validate the results obtained for the single-pollutant case.

2. Experimental

2.1. Photocatalyst preparation

Photocatalyst preparation was performed under solvothermal conditions according to the previously reported procedures [20,27,28]. Briefly, synthesis of the {0 0 1} sample was made solvothermal from 17 cm^3 of titanium *tert*-butoxide in the presence of 3.4 cm^3 of 50% wt. HF solution and 30 cm^3 of *n*-butanol. All substrates were mixed and placed inside a 200 cm^3 Teflon-lined reactor at 210 °C for 18 h. Sample exposing {1 0 0} facets was prepared in a two-step reaction, starting from the 1 g of commercial TiO_2 P25, which was etched at 120 °C for 20 h using 40 cm^3 of 10 M NaOH solution inside the 100 cm^3 reactor. The obtained Na-titanate product was washed with water until pH equaled 10.5 and immediately separated into two equal parts. Each part was mixed with 100 cm^3 of water inside the 200 cm^3 reactor and was left to react at 210 °C for 24 h. Sample exposing {1 0 1} facets was prepared analogically to the {1 0 0}, except that 8.5 M solution of KOH was used in the first reaction, and the obtained K-titanate product was washed until pH reached approximately 7. In the second step, 0.4 g of the dried K-precursor was mixed with the 100 cm^3 of NH_4OH/NH_4Cl buffer with concentrations of 0.3/0.3 M (pH approximately 9) and left to react at 210 °C for 16 h. All prepared samples were centrifuged, washed with water 4 times, dried, and hand-grounded in the agate mortar before further characterization and photocatalytic studies.

2.2. Photocatalyst characterization

Obtained photocatalysts were investigated concerning their crystal structure, diffuse reflectance UV/Vis absorbance spectra (DR-UV/vis), Brunauer-Emmett-Teller surface area (BET), and morphology. The crystal structure was analyzed based on the X-ray diffraction pattern (XRD) in the 2Θ range 10–80°, collected using Rigaku MiniFlex diffractometer with the scan speed and step being 2°·min^{-1} and 0.05° respectively. The crystallinity of the prepared samples was analyzed using highly crystalline NiO as an internal standard. The DR-UV/vis absorbance spectra were recorded using ThermoFisherScientific Evolution 220 spectrophotometer with $BaSO_4$ as a standard in the λ range between 200 and 800 nm. The Fourier-transformed infrared (FTIR) absorption spectra were measured using a Thermo Fisher Scientific Nicolet iS10 spectrometer in the wavenumber from 1500 to 4000 cm^{-1}. Before measurements, the analyzed sample was mixed with the KBr, and the pellet was made using a hydraulic press. The BET surface area was analyzed based on the N_2 adsorption isotherm in the 77.15 K between the $p/p_0 = 0.05$ and 0.3, and the samples were degassed at 200 °C for 2 h prior to the measurement. The morphology of the samples was observed under the FEI Quanta FEG 250 scanning electron microscope (SEM). The surface composition of the samples was analyzed based on the X-ray photoelectron spectroscopy (XPS) measurements performed with the PHI 5000 VersaProbe (ULVAC-PHI) spectrometer.

2.3. Photocatalytic degradation analysis

Firstly, the photocatalytic degradation experiments in the presence of faceted TiO_2 were performed in 15 cm^3 reactors at constant temperature (25 °C), with magnetic stirring using a high-pressure Hg lamp as an irradiation source with 15 mW•cm^{-2} of UVA flux at the reactor border. Moreover, control experiments were made using commercial TiO_2 P25 as a standard material. These experiments were performed for a single solution of each pollutant (with the initial concentration of 20 mg·dm^{-3} for acetaminophen, ibuprofen, and phenol and 14 mg·dm^{-3} for carbamazepine), as well as for the mixture of examined pharmaceuticals. Before irradiation, each solution was stirred for 30 min in the dark to ensure adsorption equilibrium between the photocatalyst and the organic pollutant. After this time, irradiation with light was started, and sam-

ples were taken at given intervals and filtered through syringe filters (φ = 0.2 μm) for the removal of photocatalyst particles. Furthermore, the pharmaceuticals mixture degradation using facet-engineered photocatalysts was performed and the stability of the photocatalyst was analyzed in the subsequent cycles of degradation. Moreover, the trapping experiments in the presence of the active species scavengers were performed to discuss their role in the degradation process (5 mmol•dm^{-3} of isopropanol as •OH scavenger, 1 mmol•dm^{-3} of benzoquinone as $\bullet O_2^-$ scavenger or 5 mmol•dm^{-3} of ammonium oxalate as h^+ scavenger). Additionally, the relative •OH generation ability was tested using 50 μmol•dm^{-3} coumarin solution and determined the initial formation rate of 7-hydroxycoumarin for the obtained photocatalyst samples. Quantification of the 7-hydroxycoumarin was performed based on the calibrated emission intensity at 454 nm after exciting solution with the 332 nm wavelength using a Shimadzu RF-6000 spectrofluorometer. Finally, degradation experiments using an alternative set-up with a 300 W Xe lamp were performed to discuss the possible effect of light. During these experiments, the measured UVA flux at the reactor border was 25 mW•cm^{-2}. Besides the coumarin-based tests, the concentration of all pollutants was evaluated with the high-pressure liquid chromatography method using a Shimadzu LC-6A system equipped with a pump (LC-20 CE), autosampler (SIL-20AHT) and diode array detector (SPD-M20A). During all measurements, the Phenomenex Kinetex C-18 column (150 × 4.6 mm, 2.6 μm) was used for separation. An isocratic method was used for every examined pharmaceutical, but flow rate, the composition of the eluents and wavelengths of detection varied depending on the compound; details are presented in Table 1. Mineralization of the pharmaceuticals was determined as a removal of the total organic carbon (TOC) and measured using a Shimadzu TOC-L analyzer. Degradation rate constants were calculated assuming a first-order reactions model. In the case of a visible change in the observed rate in the initial and late part of the process, the final rate constant was calculated as a mean between different linear regions.

2.4. Computational details and structure-activity relationship

Computational studies of the analyzed pharmaceutical molecules were performed with the density functional theory (DFT) calculations using Orca 5.0.3 software [29,30]. All calculations were performed using the hybrid exchange-correlation B3LYP functional [31] with aug-cc-PVDZ basis set. Such a combination was recently reported to be reliable in predicting some molecule parameters, such as a dipole moment, under a reasonable computational time [32]. Each molecule was optimized to its relaxed geometry, and the true energy minimum was confirmed with the vibrational frequencies (no negative frequencies) analysis. Geometry optimization was followed with the analysis of HOMO and LUMO orbitals for each molecule. All computations were performed using the CMCP model of continuum solvation.

Based on the performed calculations, a set of parameters representing each molecule was obtained and used for further structure-activity analysis. Specifically, the HOMO and LUMO energies, HOMO-LUMO gap, dipole moment, total Gibbs energy, chemical potential, electronegativity, chemical hardness, softness, and electrophilicity index were selected to represent each pollutant. The values of HOMO and LUMO energies (E_{HOMO} and E_{LUMO}), HOMO-LUMO gap (ΔE), dipole moments (d), and total single-point energies (G) were obtained directly from the computed results. The chemical potentials (μ), electronegativities (χ), absolute hardness (η), softness (S), and electrophilicity indices (ω) were calculated for each molecule based on the original definitions by Parr and Pearson [33,34] under the assumptions of Koopman theorem [35] with further improvement by Tozer and De Proft concerning the exact η value [36]. The final equations are:

$$\mu = \frac{(E_{LUMO} + E_{HOMO})}{2} = -\chi \quad (2)$$

$$\eta = \frac{(E_{LUMO} - E_{HOMO})}{2} + E_{HOMO} + I = \frac{1}{S} \quad (3)$$

$$I = E_{N-1} - E_N \quad (4)$$

$$\omega = \frac{\mu^2}{2\eta} \quad (5)$$

where I is vertical ionization potential, E_N is the energy of the considered molecule and E_{N-1} is the energy of the same molecule with one less electron.

3. Results and discussion

3.1. Photocatalyst structure and properties

Characterization of the prepared photocatalysts was started from the analysis of their crystal structure and UV–vis absorption properties, as presented in Fig. 1. All samples are single-phase TiO_2 with the reflections corresponding to the anatase crystal structure. Moreover, in the case of sample {0 0 1} prepared with the addition of HF as a stabilizing agent, visible broadening of the (0 0 4) and (1 0 5) reflections can be observed, which results from the thickening of the nanocrystals along the c crystallographic direction.

Simultaneously, this sample had about 20% wt. of the amorphous phase, as shown in Table 2, based on the additional measurements with NiO as the internal standard. Noteworthy, the crystallinity of the TiO_2 can influence its photocatalytic activity, however it was shown previously that its effect is not significant in phenol degradation (crystallinity between ~10–85%) [37]. Furthermore, our recent study has also shown that particularly in the case of different samples with exposed {0 0 1} facets, their ability to degrade phenol is not connected with the presence of amorphous phase content (crystallinity between ~34–81%), but depend mostly on the surface development and surface defects [20]. In this regard, the determined 20% presence of the amorphous phase is not expected to be decisive for the comparison of the samples. Comparing to the {0 0 1} exposed one, samples {1 0 0} and {1 0 1} did not show visible amorphous phase content.

Furthermore, as shown in Fig. 1b, the absorbance spectra of all samples are similar and negligible below 400 nm. The bandgap energies are shown in Fig. 1c and were about 3.22 eV for all samples, which is a value characteristic of the pure anatase structure. Finally, the SEM images presented in Fig. 1d confirmed morphology differences, characteristic for each exposed facet (rectangular plates in the case of {0 0 1} exposition, rectangular rods for {1 0 0} and octahedrons in the case of {1 0 1}). Corresponding BET surface areas are shown inset of SEM images.

Table 1
HPLC methods parameters.

Parameter	Acetaminophen	Carbamazepine	Ibuprofen	Phenol
Wavelength (nm)	244	285	219	272
Flow rate (cm^3·min^{-1})	0.8	1.5	0.5	0.3
Injection volume (μL)	10	10	10	10
Temperature (°C)	45	45	45	45
Mobile phase (v/v)	MeOH/H_2O/HCOOH 30/69.9/0.1	H_2O/ACN/H_3PO_4 68/31.6/0.4	ACN/H_2O/H_3PO_4 70/29.5/0.5	ACN/H_2O/H_3PO_4 70/29.5/0.5

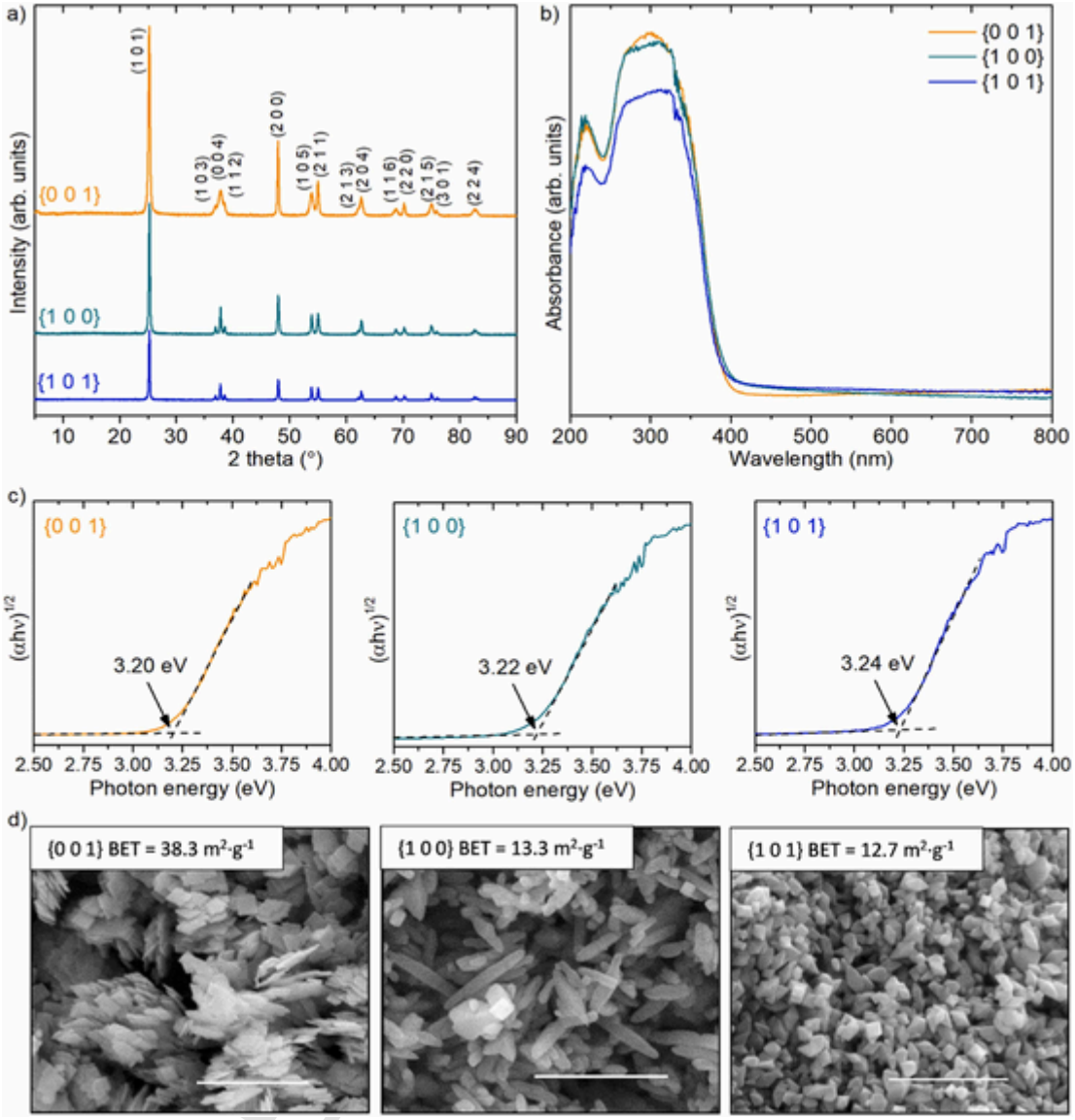

Fig. 1. Basic characteristics of the obtained photocatalysts, including XRD patterns (a), UV–vis absorption spectra (b), calculated bandgap values (c), and SEM morphology of the samples with obtained BET surface areas (d). Scale bars are 1 μm.

Table 2
Summation of the XPS results and crystallinity of the prepared samples (LOD stands for "*limit of detection*").

Sample	Ti^{4+} (485.5 eV)	Ti^{3+} (486.5 eV)	F_{ads} (684.5 eV)	F/Ti	Amorphous content
{0 0 1}	100%	Below LOD	100%	0.19 at.	20%
{1 0 0}	100%	Below LOD	Below LOD	-	Below LOD
{1 0 1}	100%	Below LOD	Below LOD	-	Below LOD

Furthermore, the surface hydroxylation of the samples was analyzed based on the performed FTIR analysis, as presented in Fig. 2. The presence of adsorbed water is observed for all samples, with a broad peak in the range of 3650–3000 cm^{-1} and a sharp one at 1635 cm^{-1}, corresponding to the stretching and bending vibrations of the H_2O [38]. Noteworthy, sample {1 0 0} showed visible enhancement of the absorption near 3100 cm^{-1}, suggesting that some amount of H_2O is bound stronger to the surface [39].

This is in some agreement with the known stabilization of the {1 0 0} facets through increased hydroxylation [40], which might suggest stronger TiO_2-H_2O interactions. Nevertheless, the overall amount of adsorbed H_2O is similar for {1 0 0} and {1 0 1} samples and is only slightly higher for the {0 0 1} one, as observed for the 1635 cm^{-1} signal. Since the analysis was performed for the controlled, similar amount of samples, this is in agreement with the determined surface development, which should affect the number of possible adsorption sites. Therefore, surface hydroxylation seems similar between the samples, with absorption proportional to the surface development.

Considering the possible surface defects, XPS analyses were performed, and the results are summarized in Table 2. As observed, no surface Ti^{3+} was noticed for the prepared samples, suggesting the absence of structural surface defects. Combined with the UV–vis spectra presented in Fig. 1, this shows that the overall structure is defect-free. Moreover, in the case of samples {1 0 0} and {1 0 1}, their overall characteristics are very similar, and therefore, differences in the exposed facets are expected to be the main factor affecting their photocatalytic performance. Some differences are observed only in the case of the sample with exposed {0 0 1} facets. However, it should be noted that the

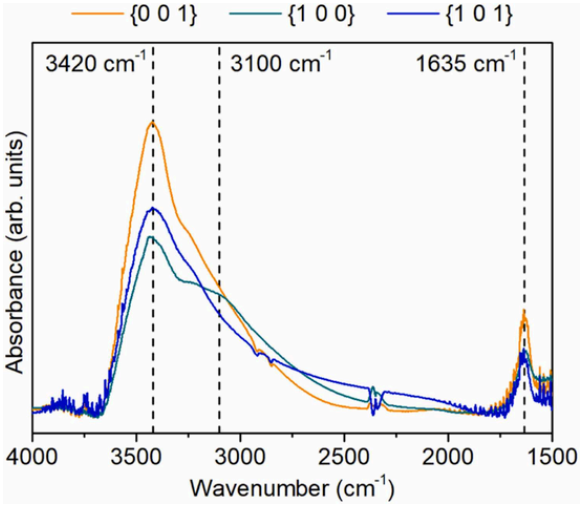

Fig. 2. FTIR spectra of the prepared TiO_2 samples.

preparation route of this sample is based on the previously optimized procedure [20]. In this regard, it should be a good representative of the material exposing the majority of the {0 0 1} facets. The final noteworthy observation for this sample is the presence of surface-adsorbed fluorine, which is typical for the materials prepared in the presence of HF. The calculated atomic ratio between F/Ti is 0.19, which might influence the electronic structure of the (0 0 1) surface. However, it is expected that partial fluorination of the {0 0 1} facets is inhibiting to their photocatalytic activity [41–43]. Particularly, 2D samples prepared at very analogical conditions have not shown a negative effect of surface fluorination between F/Ti = 0.13 and 0.18 [20]. Moreover, the final activity of these samples could be improved with a suitable post-treatment. However, these effects are reported to be within the range of a 20% activity increase [24,44]. As it will be shown later, differences in the activity observed between prepared samples are a few times larger than this, suggesting the predominant effect of the exposed facet.

3.2. Degradation study of single pharmaceutical compounds

Obtained materials were analyzed for photocatalytic degradation of selected pharmaceuticals; carbamazepine (CBZ), ibuprofen (IBU) and acetaminophen (ACT) in water to determine possible interactions between their structure and the exposed facet of the photocatalyst. Furthermore, the degradation of phenol (PHE), a widely used model organic pollutant, as well as TiO_2 P25 as a standard photocatalytic material, were performed as control experiments for other analyses. As shown in Fig. 3 and Table 3, all of the TiO_2 nanostructures can induce degradation of the tested compounds, while the spontaneous photolysis is low. Furthermore, visible differences between specific pollutant-photocatalyst reactions are noticeable. First of all, carbamazepine and ibuprofen appear to be more prone to adsorb on the photocatalyst surface in the absence of light. This is especially visible for ibuprofen and is in agreement with its expected anionic form in neutral conditions (pKa = 5.2), which can promote its interactions with the TiO_2 surface.

These differences, observed without light, are generally followed by the degradation efficiency under the UV–vis light, with the highest rates observed for carbamazepine and ibuprofen, followed by acetaminophen and lastly phenol photodegradation. In all cases, sample exposing {1 0 1} facets exhibit the highest activity, while nanosheets exposing {0 0 1} revealed the lowest photoactivity. The weak performance of the sample with exposed {0 0 1} facets is even more noticeable when considering its relatively large surface area compared to the remaining two (approx. 3 times larger). This is in agreement with our recent studies, showing higher activity of the {1 0 1} facets than {0 0 1} for phenol degradation [19,20]. However, it especially confirms that this observation is not limited to phenolic compounds and could also be expected for other water pollutants. Furthermore, it is also in agreement with the control experiments of the •OH radicals generation, using 7-hydroxycoumarin (7-OHC) as the fluorescent probe [45], directly connecting observed pharmaceutical degradation rates with the ability to generate hydroxyl radicals (7-OHC generation rates were 36 nM•min^{-1} for {0 0 1} sample, 52 nM•min^{-1} for the {1 0 0} and 74 nM•min^{-1} for the {1 0 1} one). Noteworthy, the sample exposing{1

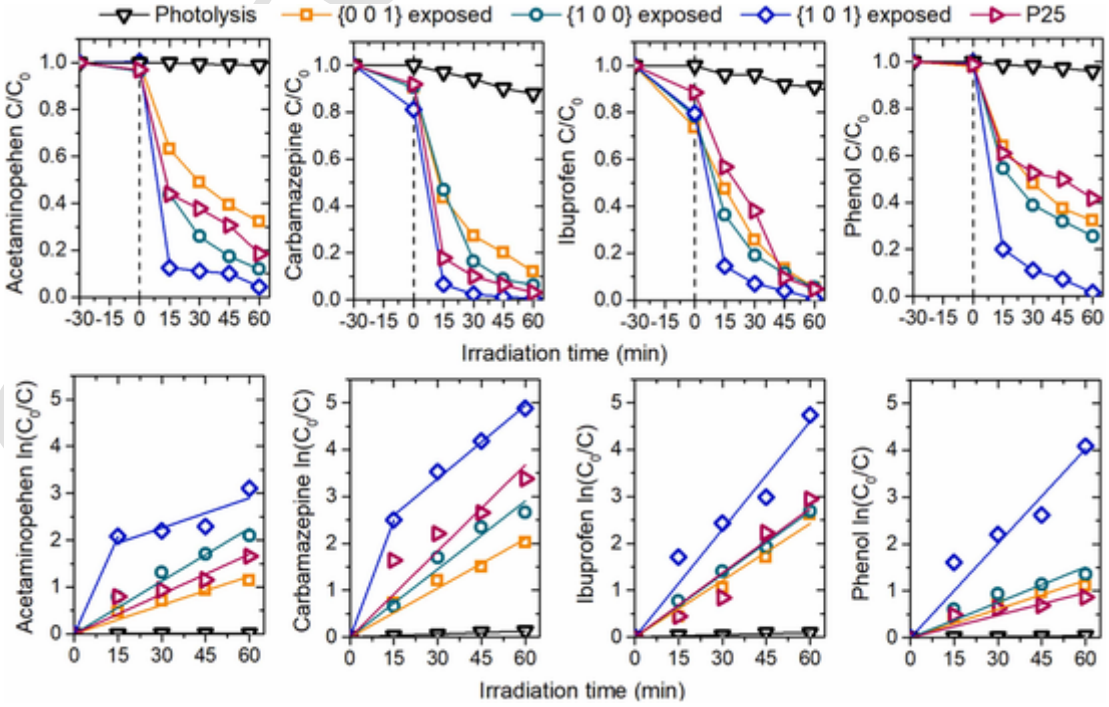

Fig. 3. Observed photocatalytic degradation of the acetaminophen (ACT), carbamazepine (CBZ), ibuprofen (IBU) and phenol (PHE) over prepared TiO_2 samples.

Table 3
Detailed values of the observed rate constants and initial concentrations.

Compound	Carbamazepine	Ibuprofen	Acetaminophen	Phenol
C_0 (mg•dm^{-3})	13.0	20.6	19.5	18.9
k_0 (s^{-1})	0.36•10^{-4}	0.28•10^{-4}	0.03•10^{-4}	0.11•10^{-4}
$k_{\{0\ 0\ 1\}}$ (s^{-1})	5.82•10^{-4}	6.73•10^{-4}	3.42•10^{-4}	3.40•10^{-4}
$k_{\{1\ 0\ 0\}}$ (s^{-1})	8.06•10^{-4}	7.45•10^{-4}	6.26•10^{-4}	4.19•10^{-4}
$k_{\{1\ 0\ 1\}}$ (s^{-1})	18.20•10^{-4}	12.78•10^{-4}	13.33•10^{-4}	11.19•10^{-4}
k_{P25} (s^{-1})	10.20•10^{-4}	7.62•10^{-4}	4.73•10^{-4}	2.68•10^{-4}

0 1} facets revealed higher photocatalytic activity than commercial TiO_2 P25, despite a few times lower surface area.

Degradation tests were followed by the measurements of total organic carbon (TOC) before and after 60 min of the process to verify the possible mineralization of the target compound. As shown in Fig. 4, the observed removal of the organic carbon between the samples is in general agreement with their degradation rates and follows the order {1 0 1} > {1 0 0} > {0 0 1}. The only exception is carbamazepine degradation over the {1 0 0} facets, which achieved the highest TOC removal.

However, the value is very close to the {1 0 1} one. Regarding the pollutant type, some discrepancy might be seen between the observed degradation rate and final TOC removal, which generally is quite high for phenol and acetaminophen. This might result from the fact that their molecules are relatively smaller than carbamazepine and ibuprofen, which might promote their faster breaking into CO_2, despite relatively slow transformation at the beginning of the process (number of carbon atoms per one molecule is 15 for CBZ, 13 for IBU, 8 for ACT and 6 for PHE).

Finally, it is also visible that the mineralization of ibuprofen is visibly slower than other pollutants, suggesting that the degradation rates of further transformation products are low for this compound. Relatively low TOC removal during the ibuprofen degradation by TiO_2 was reported previously [46,47], and generally, additional reagents such as ozone are known to enhance the degradation of possible intermediates [48]. Compared to the facet-engineered TiO_2 samples, commercial TiO_2 P25 revealed higher TOC reduction efficiency only for IBU degradation. This suggests that either higher surface development or charge carriers separation might be crucial for IBU mineralization (P25 is composed of both rutile and anatase phases and therefore, improved separation of the generated e^- and h^+ between both components is possible in this case).

3.3. Analysis of facet-pollutant interactions with respect to pollutant structure

Obtained results showed that regardless of the pollutant structure, the {1 0 1} facets are the most active, in each case recreating the same trend as previously observed for phenol [24]. Therefore, the activity order of the exposed facets is not dependent on the exact pollutant structure. Moreover, since ibuprofen is present in its anionic form during the process (pKa = 4.91), even a specific charge on the pollutant molecule seems to be less important, not influencing the overall trend. In this regard, experimental data was compared with the modeled results obtained using a previously optimized Eq. (1). Details of the model parameter, based on the studies focused on the analysis of the TiO_2 surfaces [24–26], are presented in Table 4.

However, as shown in Fig. 5a, such rate constants, predicted without considering the pollutant structure, do not follow the experimental results strictly. Furthermore, some series fit better to the initial model when grouped by the pollutant type, while ibuprofen and carbamazepine show the highest deviation (Fig. 5b). Although the exposed TiO_2 crystal facet primarily determines the overall activity, the prediction of the degradation rate without taking into account pollutant structure can lead to relatively high error, especially when comparing the degradation of different compounds. Therefore, identification of the pollutant-specific features that determine the observed activity might be desirable to better describe TiO_2-pollutant interactions.

In this regard, to describe the effect of the pollutant structure, the initial model (1) was rearranged to focus on the $n_{trap}/n_{pollutant}$ term since all others are either constant (k_0) or depend strictly on the photocatalyst nature and not on the pollutant (E_{surf} and E_{trap}). Therefore, the analyzed relation could be presented as described in Eq. (6).

$$\frac{k - k_0}{E_{surf} \cdot \left(e^{\frac{0.02766 \cdot E_{trap}}{kT}} - 1 \right)} = A_1 \cdot \left(\frac{n_{trap}}{n_{pollutant}} \right)^C \quad (6)$$

where the left side of the equation is known, while A_1 and C are new fitted factors. It should be noted that previously the C was found to be ½ in the case of phenol degradation, however it is not obvious if this will be true for other pollutants as well. Therefore, the analysis was started by considering C = ½; 1 and 2 and looking for possible A_1 values.

Fig. 6 presents the obtained relations, showing that overall the C = 1 gives the best accuracy between all pollutants. In this regard, the values of A_1 fitted for this case (C = 1) and presented in Table 5 were taken for further analysis.

The actual pollutant structure-activity analysis was started with computational simulations of each pollutant under the DFT theory level

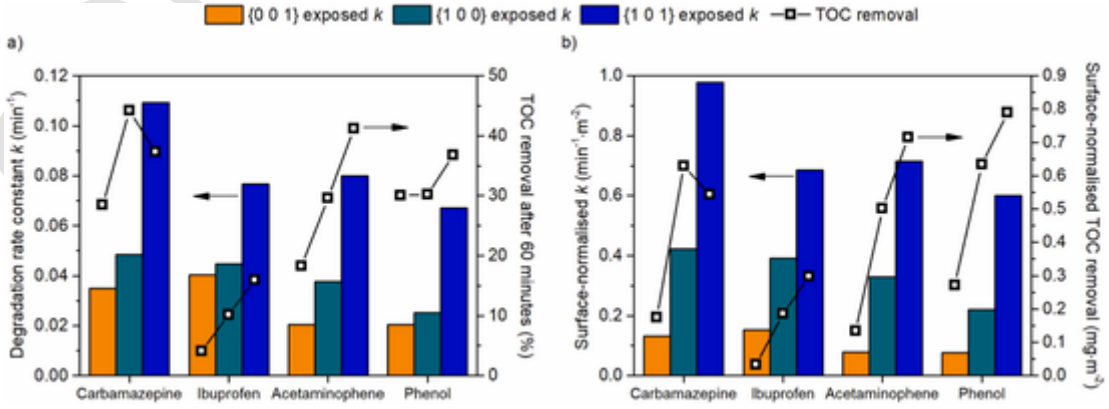

Fig. 4. Calculated degradation rate constants and removal of the total organic carbon (TOC) for the investigated compounds in the presence of different TiO_2 nanostructures; (a) as observed and (b) after normalization with the surface area of the photocatalyst. Column order from left to right match the one in the legend.

Table 4
Detailed values introduce to the initial model, considering different TiO_2 facets.

Facet	E_{surf} (J•m^{-2})	E_{trap} (J)	n_{trap} density (m^{-2})	A	B
{0 0 1}	0.90	$0.77 \cdot 10^{-19}$	$6.96 \cdot 10^{18}$	$3.327 \cdot 10^{-4}$	0.02766
{1 0 0}	0.53	$2.30 \cdot 10^{-19}$	$9.25 \cdot 10^{18}$		
{1 0 1}	0.44	$3.80 \cdot 10^{-19}$	$1.03 \cdot 10^{19}$		

with CMCP solvation model. The optimized structures of each molecule in their dominant aqueous form (ibuprofen as an anion) are presented in Fig. 7, together with their HOMO and LUMO maps and energies. Based on these results, a set of global reactivity predictors [49] was determined, as described in the experimental section. The exact values of each predictor are shown in Table 6. Based on the values presented in Table 6, the correlation between the predictors and A_1 value, determined as a slope from Fig. 6 for $C = 1$, was studied assuming simple linear relation.

The values of the observed R^2 parameters for different A_1 expressions, including single predictor or their combinations and squared values, are presented in Table 7. The full analysis included each predictor independently, as well as their interactions (multiplication of two predictors) and squared values. Obtained results have shown a very strong correlation between the fitted A_1 parameter and the chemical softness/hardness, as well as the HOMO-LUMO energy difference (ΔE). At this point, it should be noted that these predictors are directly related (Eq. (3) in the experimental section), so similarities are not unexpected.

Concerning the hardness/softness relations, the softness value is an inverse of the hardness and the correlation is slightly more accurate for the hardness (η). As a result, it is observed that "harder" compounds react faster with the photocatalyst. The same relation is true for the higher HOMO-LUMO gap. In both cases, the best accuracy is observed for the squared values of η and ΔE, presented in Fig. 8.

Ultimately, we propose that within the investigated range of η and ΔE, A_1 can be described using both of these predictors (Eqs. (7) and (8)), considering their values in J:

$$A_1 = 2.73231 \cdot 10^{33} \cdot \eta^2 - 9.21375 \cdot 10^{-5} \quad (7)$$

$$A_1 = 6.86473 \cdot 10^{32} \cdot \Delta E^2 - 1.48052 \cdot 10^{-4} \quad (8)$$

For both of the possible A_1 equations, the final model might be visibly improved, as shown in Fig. 9 for the case of η^2 relation (combination of Eq. (7) with Eq. (1)). Here, the only point that visibly stands out is ibuprofen degradation over {1 0 1} sample. However, it can be noticed that this is a special case. As mentioned, in the neutral conditions,

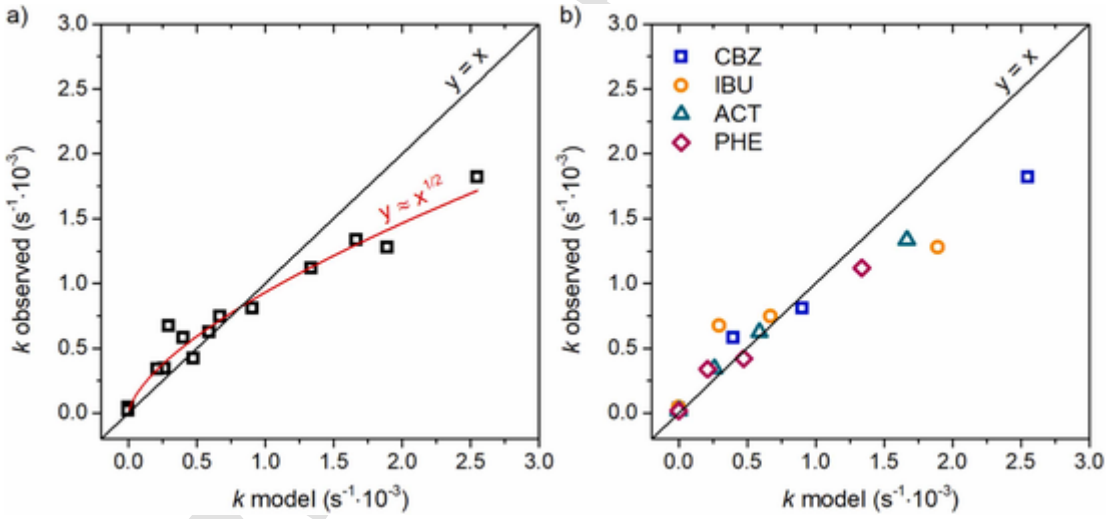

Fig. 5. Results of modeling the degradation rate constant based on a model developed for phenol degradation over different TiO_2 facets (a); as well as their further division with respect to the pollutant (b).

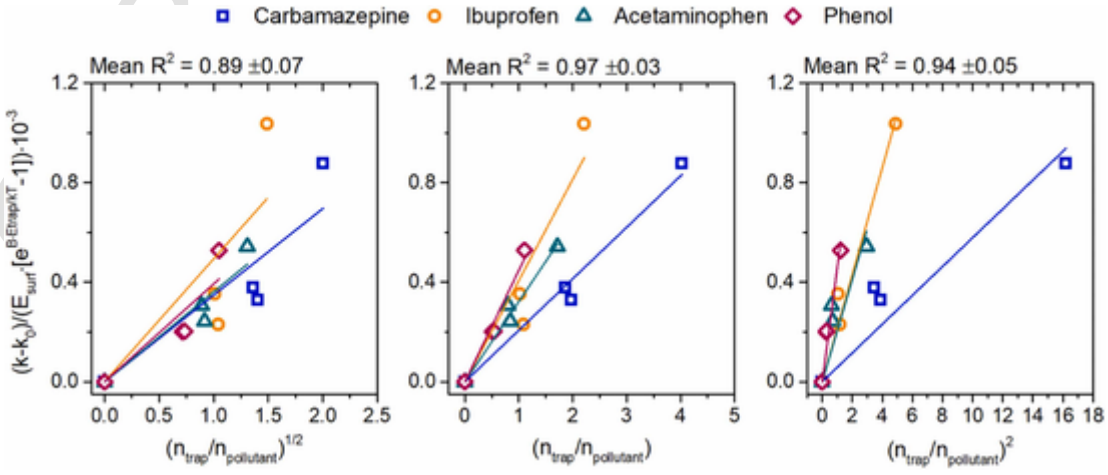

Fig. 6. Linear relations between the pollutant-independent part of the model (OY axis) and the ratio between the number of photocatalyst trapping sites and the number of pollutant molecules, including different C exponents.

Table 5
Detailed values of the A_1 parameter obtained for $C = 1$.

	Carbamazepine	Ibuprofen	Acetaminophen	Phenol
A_1	$2.06889 \cdot 10^{-4}$	$4.07053 \cdot 10^{-4}$	$3.22663 \cdot 10^{-4}$	$4.48345 \cdot 10^{-4}$

ibuprofen is present in its anionic form, while {1 0 1} facets are specifically reductive and prefer to accumulate electrons during the photocatalytic process, in contrast to both {0 0 1} and {1 0 0} [25]. In this regard, under UV light irradiation, electrostatic interactions might specifically hinder the process for this particular case, which is observed as k being visibly lower than predicted.

However, it should also be noted that for pollutants with possibly low values of η and ΔE, for example dyes, the introduction of Eqs. (7) and (8) could result in negative A_1 values, which is not reasonable. In this regard, for such compounds, modified relations (9) and (10) could be used.

$$A_1 = 1.9263 \cdot 10^{33} \cdot \eta^2 \quad (9)$$

$$A_1 = 4.04836 \cdot 10^{32} \cdot \Delta E^2 \quad (10)$$

This is further justified by control experiments of methyl orange (MO) degradation. MO is known to have a small HOMO-LUMO gap of 2.01 eV, which under the Koopman theorem, corresponds to the chemical hardness value of about 1.005 eV. Therefore, as shown in Table 8, the introduction of Eqs. (7) and (8) results in a negative value of A_1 and, in consequence, a negative value of k, which is meaningless. On the other hand, scaling the relation down to (0, 0) with Eqs. (9) and (10) results in the final predicted k being already close to the experimental results. Moreover, it is noteworthy that both predicted and observed rate constants are the order of magnitude lower than in the case of other compounds. This is in agreement with the general trend that lower η or ΔE should result in slower degradation.

3.4. Interpretation of the model

The final model shows that the observed photocatalytic degradation rate of different organic pollutants in water depends mostly on three factors: (i) the ratio between surface trapping centers of the photocatalyst and the number of pollutant molecules, (ii) the trapping energy of charge carriers on the photocatalyst surface and (iii) chemical hardness, or alternatively HOMO-LUMO energy gap, of the degrading pollutant. In each case, an increase in the numerical value of the factor results in an increase in the observed degradation rate constant. The first one of the factors is right now well understood during the photocatalytic processes, and an increase of the k with an increasing number of the surface active centers is expected. Furthermore, we have recently reported that for a faceted TiO_2, the probability of charge carriers trapping on the surface, defined with trapping energy, is crucial for the degradation of organic compounds. Therefore, the combination of factors (i) and (ii) describes the probability of charge carriers trapping at the surface and the actual number of possible trapping centers per number of reacting molecules, and their further interpretation seems unnec-

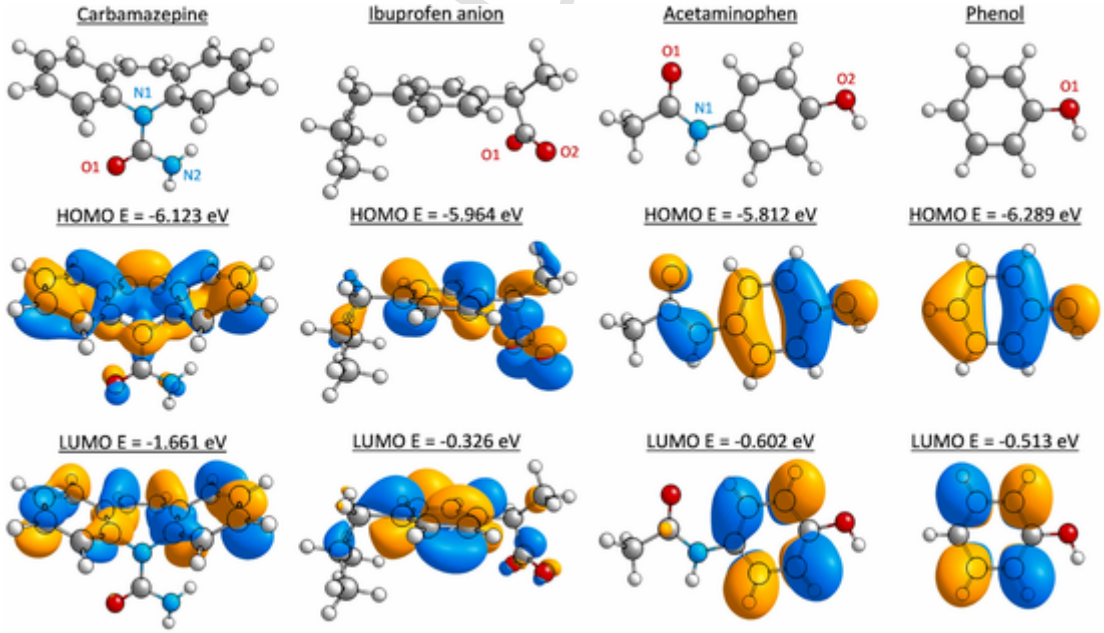

Fig. 7. Visualization of the optimized geometry for each pollutant, as well as their HOMO and LUMO maps and corresponding energies. Grey, white, cyan and red spheres are C, H, N and O atoms, respectively. In the case of ibuprofen, only the geometry of R enantiomer is shown since no significant difference was observed for the S structure, however the HOMO and LUMO energies are presented as mean.

Table 6
Detailed values of the reactivity predictors describing each of the analyzed molecules.

Compound	G (Ha)	d (D)	E_{HOMO} (eV)	E_{LUMO} (eV)	ΔE (eV)	μ (eV)	χ (eV)	η (eV)	S (eV)	ω (eV)
CBZ	-763.22	6.09	-6.123	-1.661	4.462	-3.892	3.892	2.046	0.489	3.702
ACT	-515.28	7.29	-5.812	-0.602	5.210	-3.207	3.207	2.475	0.404	2.077
PHE	-307.34	1.82	-6.289	-0.513	5.775	-3.401	3.401	2.766	0.362	2.091
[IBU]⁻ (mean)	-655.92	18.36	-5.964	-0.326	5.638	-3.145	3.145	2.653	0.377	1.864
[IBU]⁻ R	-655.92	18.28	-5.959	-0.327	5.632	-3.143	3.143	2.649	0.378	1.864
[IBU]⁻ S	-655.92	18.45	-5.970	-0.325	5.645	-3.147	3.147	2.657	0.376	1.864

Table 7
Detailed values of the R^2 parameters describing the linear correlation between the determined predictors (independent and including 2-factor interactions) and observed A_1 values.

R^2 matrix	G	d	E_{HOMO}	E_{LUMO}	ΔE	μ	χ	η	S	ω
Single	0.56	0.02	0.05	0.81	**0.99**	0.54	0.54	**0.98**	**0.96**	0.76
G	0.59	< 0.01	0.57	0.85	0.23	0.73	0.73	0.20	0.77	0.83
d		0.09	0.02	0.75	0.04	< 0.01	< 0.01	0.05	< 0.01	0.06
E_{HOMO}			0.05	0.79	**0.97**	0.31	0.31	**0.97**	0.84	0.70
E_{LUMO}				0.79	0.78	0.79	0.79	0.77	0.83	0.79
ΔE					**0.99**	0.45	0.45	**0.99**	0.74	0.60
μ						0.56	0.56	0.61	0.83	0.72
χ							0.56	0.61	0.83	0.72
η								**0.99**	0.02	0.56
S									**0.95**	0.82
ω										0.76

essary. However, to our best knowledge, factor (iii) is reported for the first time, and in this regard, we will discuss its interpretation further.

Firstly, it is noteworthy that compared to other studied reactivity predictors, both η and ΔE depend on the energetic stability of the pollutant when an electron is added or removed from the molecule. This is presented in Fig. 10, where additional calculations were performed for the molecules with a number of electrons $N + 1$ and all results are presented relative to the energy in the ground state. In this figure, higher points on the OY axis are less stable, indicating possibly fast subsequent transformation. Therefore, the relative stability of the investigated compounds in their N-1 state is ACT > IBU > CBZ > PHE, while in their $N + 1$ states, it goes CBZ > IBU ≈ ACT > PHE. This ordering leads to the observation that the stability of neither $N + 1$ or N-1 state correlates with the experimental degradation data. Under the Koopman theorem, this is further true for the HOMO and LUMO energies. Alternatively, η and ΔE describe the relative stability of both N-1 and $N + 1$ states together, specifically being the second derivative of the $E(N)$ function [33] or a difference between N-1 and $N + 1$ energies (please note that initially, all E values are negative and only in Fig. 10 for clarity they are presented with different signs). For example, low stability of both $N + 1$ and N-1 states for phenol results in the highest η and ΔE values, while for carbamazepine very stable $N + 1$ state decreases both predictors. In this regard, although it should be noted that the introduction of exact E values for the N-1, N, $N + 1$ states, HOMO and LUMO energies, chemical hardness calculated using Eq. (3) or as a derivative of the curve presented in Fig. 10 give a bit different results in each case, they always create a reasonable trend with the experimentally observed results. Therefore, only when the stability of both oxidized and reduced

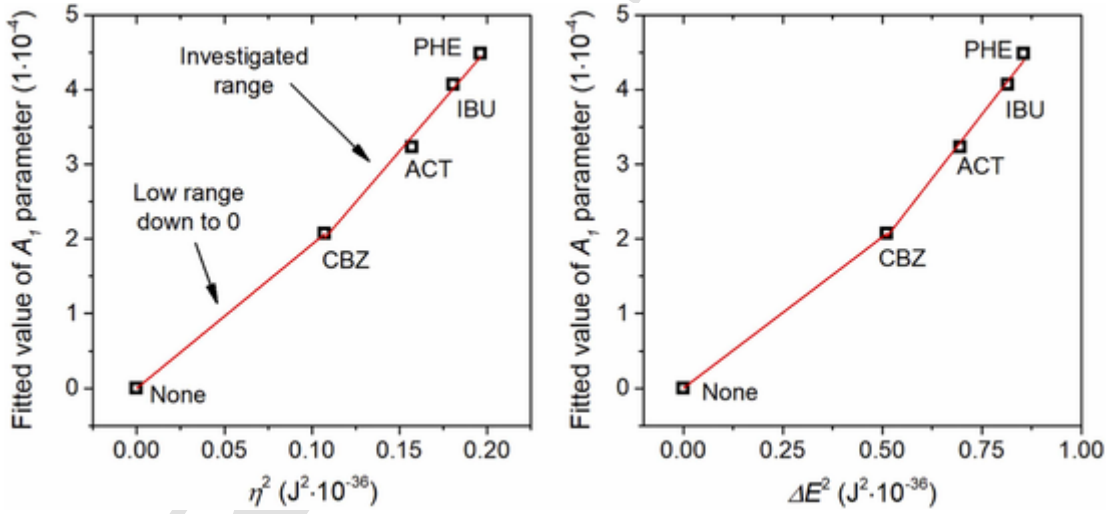

Fig. 8. Observed correlation between the fitted value of A_1 and calculated chemical hardness (η) or HOMO-LUMO energy gap (ΔE) of the pollutant.

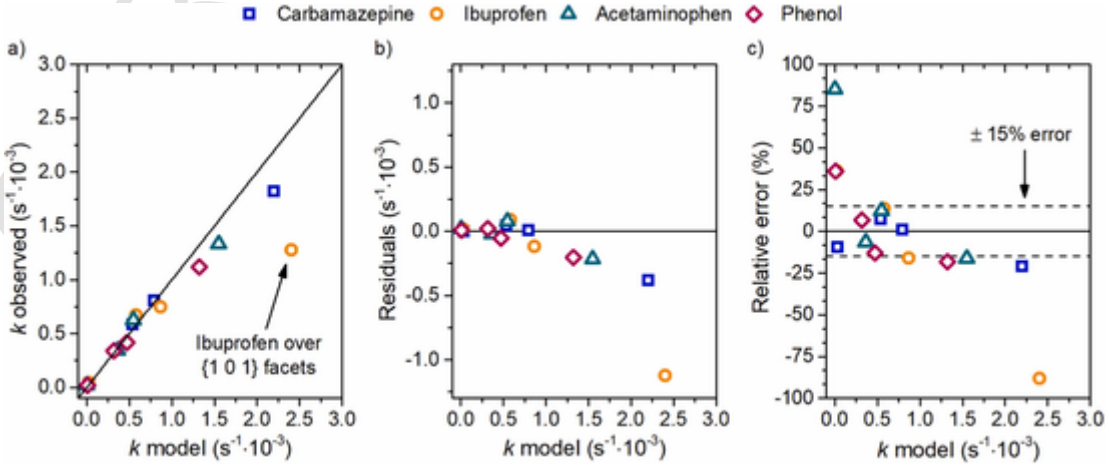

Fig. 9. Accuracy of the final model, after the introduction of the squared chemical hardness of each analyzed pollutant, presented as direct model-observation correlation (a), the absolute value of the residuals (b) and relative error (c).

Table 8
Validation of the model for methyl orange degradation. The experimental conditions were unchanged, the initial concentration of MO was about 200 μmol•dm^{-3}, similar to phenol.

Facet	MO η (J•10^{-19})	MO ΔE (J•10^{-19})	A_1Eq. (7) η^2	A_1Eq. (8) ΔE^2	A_1Eq. (9) η^2	A_1Eq. (10) ΔE^2	k_{model} η (s^{-1}•10^{-5})	k_{model} ΔE (s^{-1}•10^{-5})	$k_{observed}$ (s^{-1}•10^{-5})
{0 0 1}	1.61	3.22	-2.13•10^{-5}	-7.69•10^{-5}	4.99•10^{-5}	4.20•10^{-5}	3.43	2.89	2.81
{1 0 1}							14.7	12.4	10.05

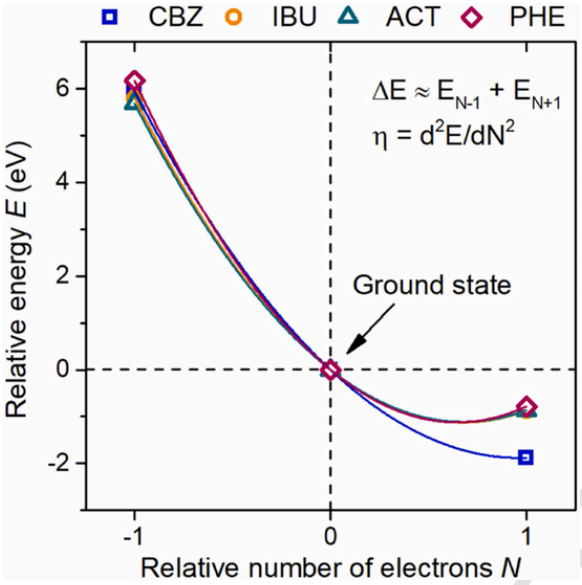

Fig. 10. Detailed results of the energy change as the function of electron number (N) obtained from the DFT simulations for investigated compounds.

molecules is considered can the final rate constant be predicted with improved accuracy.

The observations are also in agreement with the degradation mechanisms reported for different organic compounds, which usually cannot distinguish a single, well-defined degradation pathway [50–52]. Although it is commonly accepted that such processes are initiated by the hole transfer from the photocatalyst to pollutant or direct attack of •OH [53–55], it is known that electron transfer is also important for the overall process efficiency. This is either due to the involvement of the $\bullet O_2^-$, or other reduced species [56,57], in the process or due to the possible occurrence of the back reactions of organic radicals [58]. In this regard, the relative stability of the *N*-1 state for PHE, IBU and ACT agrees with the final degradation rate for these compounds, where less stable radical implies faster transformation. However, CBZ stands out from this simple relation. Based on the described results, this is correlated with the low position of the LUMO orbital and, therefore, the high stability of the $N + 1$ state of CBZ. This suggests that, especially for carbamazepine, interactions with excited electrons might be responsible for slowing down the process, either by promoting back reactions of intermediate radicals or, hypothetically, as the result of increased interactions between e^- and CBZ itself. In this regard, a detailed study on the interactions between charge carriers on the TiO_2 surface and carbamazepine, or other pollutants with a low position of LUMO orbital, might give a better insight into how the degradation process differs compared to the phenolic compounds. The differences are expected since the simple position of the HOMO orbital, corresponding to the oxidized radical state in the initial part of the process, cannot explain the lower degradation rate of CBZ, observed independently for all three investigated TiO_2 facets.

3.5. Degradation of the pharmaceuticals mixture

Finally, obtained photocatalysts and TiO_2 P25 were studied in the degradation process of the pharmaceuticals mixture, including total pollutants concentrations of 50 mg·dm^{-3}, 13 mg·dm^{-3} and 5 mg·dm^{-3} (the fraction of carbamazepine, ibuprofen, and acetaminophen was 1:1:0.5). Obtained results of the degradation rate for each individual pollutant are presented in Fig. 11a in comparison with the single-pollutant system. In the case of the 50 mg·dm^{-3} mixture, the initial concentration of each pharmaceutical is the same for individual degradation tests, and the degradation rates are decreased, which is expected due to the increased total concentration of pollutants [59].

Furthermore, two main effects can be noticed when all pollutants are present together. First of all, ibuprofen degradation is almost always in favor, showing a strong preference to react in the more complex system. This is especially visible for the {1 0 0} and {1 0 1} series, which are characterized by lower surface area. Secondly, the efficiency of acetaminophen degradation is different for each photocatalyst. Interestingly, despite lowering the total concentration, ACT degradation is not increased in the case of {1 0 0} and {1 0 1} samples between the 50 mg·dm^{-3} and 13 mg·dm^{-3} mixtures. A further increase is observed only when the total concentration decrease to 5 mg·dm^{-3}.

However, in the case of the {1 0 1} sample, the process is still hindered compared to the ACT alone. These results clearly showed that there is a preference about which pharmaceutical had a "priority" to be degraded during the process, and this follows the order of ibuprofen > carbamazepine > acetaminophen. Interestingly, acetaminophen degradation can be visibly enhanced for the {0 0 1} and {1 0 0} surfaces, but only when concentration is low enough. This relation is in agreement with the observed adsorption of the pollutants on the TiO_2 surfaces, which especially favors ibuprofen and acetaminophen the least. Therefore, pre-irradiation adsorption determines the observed degradation rate when multiple pollutants are present in the solution. This implies that a sufficiently high photocatalyst surface area should be desirable to enable the efficient degradation of all pharmaceuticals. In other cases, such as ACT degradation over the {1 0 0} and {1 0 1} facets for high total concentrations, the degradation rate of some compounds might be hindered due to the preference of other pollutants to react first. Similar observations are noticed for TiO_2 P25, which showed a significant increase in the degradation rate only for the lowest concentration of the pharmaceuticals mixture of 5 mg•dm^{-3}. Therefore, when the concentration of pollutants is relatively higher (50 mg·dm^{-3} or 13 mg·dm^{-3}), the sample exposing {1 0 1} facets generally revealed the highest photocatalytic activity, especially when comparing the available surface area of samples.

Based on these results, it could also be suggested that during the actual process, a mixture of different photocatalysts might be optimized to obtain the best performance for the mixture of pollutants with the lowest concentration of 5 mg·dm^{-3}. For example, the {1 0 0} sample showed better ACT degradation than {1 0 1} with a similar surface area, but not for the CBZ and IBU. Moreover, as shown further in Fig. 11b, these photocatalytic activities are similar for all prepared samples during three subsequent cycles of degradation.

As presented in Table 9, these results are generally followed by the removal of total organic carbon (TOC), which achieved the highest values for the {1 0 1} exposing sample (18%, 31% and 51% of the removal

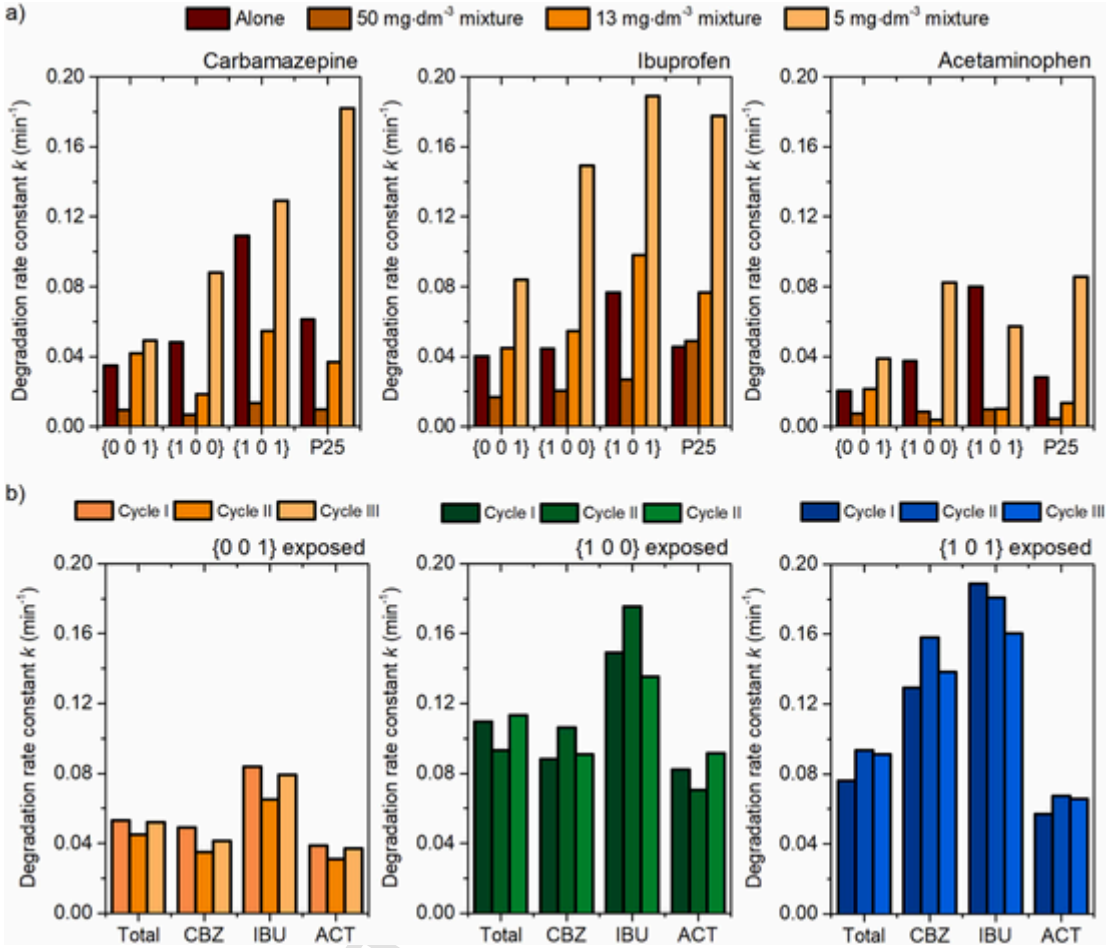

Fig. 11. Comparison of the degradation rate constants for the carbamazepine, ibuprofen and acetaminophen, over the TiO_2 photocatalysts: effect of the pharmaceuticals mixture and its concentration (a) and stability tests of the synthesized samples during degradation process of the 5 mg•dm^{-3} mixture (b). Column order from left to right match the one in the legend.

Table 9
Results of the TOC removal for the degradation of the pharmaceuticals mixtures.

Sample	Total organic carbon removal (%) after 1 h of the process						
	Mixture 50 mg•dm^{-3}	Mixture 13 mg•dm^{-3}	Mixture 5 mg•dm^{-3}				
			Cycle I	Cycle II	Cycle III	Cycle III (3 h)	Xe lamp
{0 0 1}	3	20	41	9	41	62	17
{1 0 0}	14	26	24	51	25	37	48
{1 0 1}	18	31	51	62	55	83	81
P25	11	17	69	n.d.	n.d.	n.d.	n.d.

after 1 h, depending on the concentration). Only in the case of the lowest concentration of pharmaceuticals, TiO_2 P25 achieved better TOC removal efficiency of 69%. However, after the third extended cycle of degradation (3 h), the sample exposing {1 0 1} facets achieved 83% of the TOC removal, which gives the residual value in the range of the pure water matrix (approximately 1 mg•dm^{-3}). However, it is also noteworthy that for the {0 0 1} and {1 0 0} exposing samples, higher differences were observed for the TOC removal during the cycling processes. This suggests that the final activity of these samples is more sensitive to the process conditions. Nevertheless, it doesn't influence the conclusions.

Furthermore, Fig. 12 shows observed degradation rates when specific scavengers of the active species are added to the reaction system (5 mg•dm^{-3} of pharmaceuticals). As observed, •OH, $•O_2^-$ and h^+ were found to be important for the degradation process. Nevertheless, some additional observations are noticeable. Interestingly, h^+ seems to be least important for carbamazepine degradation, especially over {0 0 1} and {1 0 0} facets. This is in agreement with the lack of correlation between CBZ degradation rate and stability of the $[CBZ]^+$ molecule, described in the previous section. On the other hand, h^+ are most important for ibuprofen removal, which also agrees with its preferred surface adsorption and negative charge. Therefore, direct h^+ transfer from the surface to the pollutant seems as a relatively important process for IBU. Finally, acetaminophen degradation is specifically sensitive to benzoquinone presence, which suggests the importance of the $•O_2^-$ radicals in its degradation process. In all cases, •OH is shown to play an important role in the photocatalytic reaction.

Finally, Fig. 13 shows the comparison between the degradation rates of the 5 mg•dm^{-3} mixture, obtained using a set-up with UV light and the alternative set-up, utilizing a lamp emitting UV–vis light. As observed, set-up with UV–vis light allowed to achieve of similar or higher degradation rates, especially affecting the transformation of CBZ and ACT over the {1 0 0} and {1 0 1} exposing samples. Noteworthy, relative degradation rates of the different pollutants over {1 0 1} sample under the UV–vis light irradiation match closely results obtained for the single compounds presented in Figs. 4 and 11a. As the nature of the photocatalyst and photogenerated active species is not expected to change depending on the UVA light source, it is shown that preferred

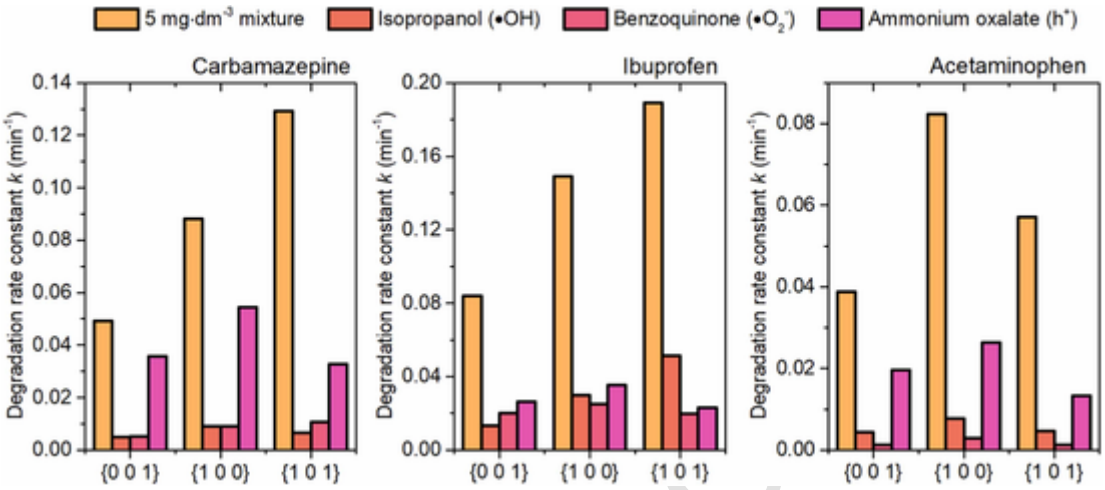

Fig. 12. Effect of the scavenger addition on the degradation rates observed for the 5 mg•dm^{-3} pharmaceuticals mixture. Column order from left to right match the one in the legend.

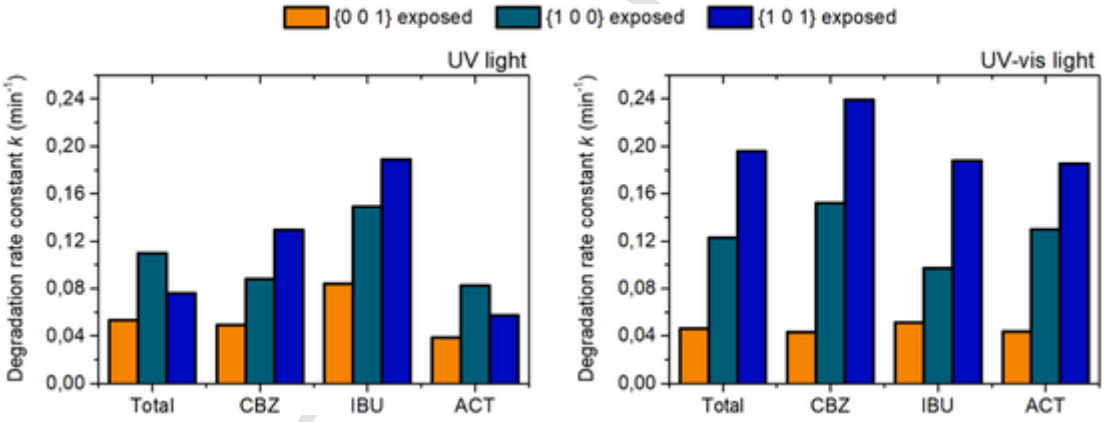

Fig. 13. Comparison of the degradation rates observed for the 5 mg•dm^{-3} using a different light sources (a), as well as scheme of the reaction set-up (b).

IBU degradation is sensitive to the parameters of the set-up itself. In this regard, two differences can be highlighted. First, utilized set-up 2 with a Xe lamp emitting UV–vis light possessed higher UVA photon flux (mW•cm^{-2}) than set-up with a UV lamp (15 mW•cm^{-2}), which generally might stimulate reaction rates. However, in this case, the effect should be uniform for all samples, which is not consistent with the observed activity for the sample exposing {0 0 1} facets. On the other hand, both photocatalytic set-ups also differ in the reactor geometry, which mostly connects with the elongated profile and slightly shorter optical length of the UV lamp reactor. From these factors, the first one seems to have a possible effect, as the long profile of the reactor results in less homogeneous mixing between the bottom and the top of the solution (this could be observed during the stabilization period of the suspension). In this regard, more homogeneous mixing and mass transfer achieved in the reactor equipped with UV–vis light (xenon lamp) might be responsible for more uniform degradation rates observed for the samples with lower surface area, resulting in the relative degradation rates being more similar to the pure compounds. Ultimately, this allowed to achieve the highest photocatalytic activity of the {1 0 1}, with a 3-times faster TOC removal, compared to a set-up equipped with a UV lamp.

4. Conclusions

The overall results present important conclusions for further studies. First of all, photocatalytic degradation of all tested emerging pollutants occurs most efficiently for anatase octahedral particles exposing {1 0 1} facets when studied independently. This proves that the efficiency of such a process depends on the density of surface trapping sites of the TiO_2, which should be high for this facet rather than its surface energy. Therefore, it confirms our previous observations made for phenol degradation, this time for a bigger set of real water pollutants with diverse chemical structures. Furthermore, after taking into account the effect of exposed crystal facets, it is observed that pollutants with higher chemical hardness (or higher HOMO-LUMO energy gap) react faster with the photocatalyst. The same correlation was not observed for the simple HOMO energy level, which would correspond to the stability of the h^+ generated organic radical, since carbamazepine significantly stands out from such a relation. This is correlated with the very low position of the LUMO orbital for CBZ, which mathematically affects value only for the η and ΔE predictors. In this regard, it is expected that detailed interactions between CBZ (or other compounds with lower LUMO position) and charge carriers on the TiO_2 surface might be different than for phenolic compounds. For the remaining compounds, the energy of the oxidized molecule gives a reasonable trend, which is in agreement with a possible process initiation by h^+. However, based on the overall results, we propose that chemical hardness or energy gap are better predictors for a diverse set of organic pollutants with different electronic properties.

Furthermore, analysis of the photocatalytic degradation of the pharmaceuticals mixture has shown that for a more complex matrix final degradation rate starts to depend on both total concentration, the pollu-

tant type and the exposed crystal facet and reactor/lamp configuration. Specifically, ibuprofen degradation was preferred, while acetaminophen degradation was hindered for the {1 0 0} and {1 0 1} facets. The preference for the degradation of ibuprofen is in agreement with the preferred adsorption during the pre-irradiation stabilization period. Therefore, the surface presence of the pollutant determines degradation efficiency, which suggests that all of the investigated pharmaceuticals react strictly on the photocatalyst surface. The results imply that for specific processes with a complex matrix, a mixture of different photocatalysts might be possibly optimized to achieve higher degradation efficiencies. Alternatively, a sufficiently high surface area of the photocatalyst or optimized process conditions might be needed to effectively induce the degradation of all compounds over a single photocatalyst.

CRediT authorship contribution statement

Szymon Dudziak: designed and conducted the experiments, carried out the DFT calculations, analyzed the data and wrote the manuscript; Agnieszka Fiszka Borzyszkowska: contributed to photocatalytic activity analyses; Anna Zielińska-Jurek: contributed to conceptualization, methodology, supervised the work, manuscript writing and editing, fund-raising, and project administration.

Declaration of Competing Interest

The authors declare that they have no known competing financial interests or personal relationships that could have appeared to influence the work reported in this paper.

Data availability

Data will be made available on request.

Acknowledgments

This work was financially supported by the Polish National Science Center with grant no. NCN 2018/30/E/ST5/00845 and grant no. 2021/43/B/ST5/02983. Furthermore, SD is grateful for the support from the Gdansk University of Technology within the program POWR.03.05.00–00-Z044/17.

References

[1] P. Paíga, C. Delerue-Matos, Sci. Total Environ. 569–570 (2016) 16.
[2] J. Liu, G. Lu, Z. Xie, Z. Zhang, S. Li, Z. Yan, Sci. Total Environ. 511 (2015) 54.
[3] E. Archer, B. Petrie, B. Kasprzyk-Hordern, G.M. Wolfaardt, Chemosphere 174 (2017) 437.
[4] M. Galus, N. Kirischian, S. Higgins, J. Purdy, J. Chow, S. Rangaranjan, H. Li, C. Metcalfe, J.Y. Wilson, Aquat. Toxicol. 132–133 (2013) 200.
[5] V. Contardo-Jara, C. Lorenz, S. Pflugmacher, G. Nützmann, W. Kloas, C. Wiegand, Aquat. Toxicol. 105 (2011) 428.
[6] M. Parolini, A. Binelli, D. Cogni, A. Provini, Chemosphere 79 (2010) 489.
[7] X. Yuan, S. Li, J. Hu, M. Yu, Y. Li, Z. Wang, Sci. Total Environ. 655 (2019) 1125.
[8] E. Donner, T. Kosjek, S. Qualmann, K.O. Kusk, E. Heath, D.M. Revitt, A. Ledin, H.R. Andersen, Sci. Total Environ. 443 (2013) 870.
[9] Z. Bielan, S. Dudziak, A. Sulowska, D. Pelczarski, J. Ryl, A. Zielińska-Jurek, Materials 13 (2020) 1.
[10] P. García-Muñoz, F. Fresno, C. Lefevre, D. Robert, N. Keller, ACS Appl. Mater. Interfaces 12 (2020) 57025.
[11] A. Grzegórska, P. Głuchowski, J. Karczewski, J. Ryl, I. Wysocka, K. Siuzdak, G. Trykowski, K. Grochowska, A. Zielińska-Jurek, Chem. Eng. J. 426 (2021) 130801.
[12] M. Kowalkińska, P. Głuchowski, T. Swebocki, T. Ossowski, A. Ostrowski, W. Bednarski, J. Karczewski, A. Zielińska-Jurek, J. Phys. Chem. C. 125 (2021) 25497.
[13] R. Mohammadzadeh Kakhki, R. Tayebee, S. Hedayat, Appl. Organomet. Chem. 32 (2018) 1.
[14] R. Tayebee, E. Esmaeili, B. Maleki, A. Khoshniat, M. Chahkandi, N. Mollania, J. Mol. Liq. 317 (2020) 113928.
[15] A. Mirzaei, L. Yerushalmi, Z. Chen, F. Haghighat, J. Hazard. Mater. 359 (2018) 516.
[16] S. Dudziak, Z. Bielan, P. Kubica, A. Zielinska-Jurek, J. Environ. Chem. Eng. 9 (2021) 105782.
[17] D. Wang, M.A. Mueses, J.A.C. Márquez, F. Machuca-Martínez, I. Grčić, R. Peralta, Muniz Moreira, and G. Li Puma, Water Res. (2021) 202.
[18] K.P. Sundar, S. Kanmani, Chem. Eng. Res. Des. 154 (2020) 135.
[19] M. Kowalkińska, S. Dudziak, J. Karczewski, J. Ryl, G. Trykowski, A. Zielińska-Jurek, Chem. Eng. J. 404 (2021) 126493.
[20] S. Dudziak, M. Kowalkińska, J. Karczewski, M. Pisarek, K. Siuzdak, A. Kubiak, K. Siwińska-Ciesielczyk, A. Zielińska-Jurek, Appl. Surf. Sci. 563 (2021) 150360.
[21] J. Chen, Y.F. Li, P. Sit, A. Selloni, J. Am. Chem. Soc. 135 (2013) 18774.
[22] M. Setvin, U. Aschauer, J. Hulva, T. Simschitz, B. Daniel, M. Schmid, A. Selloni, U. Diebold, J. Am. Chem. Soc. 138 (2016) 9565.
[23] Y.F. Li, A. Selloni, ACS Catal. 6 (2016) 4769.
[24] S. Dudziak, M. Kowalkińska, J. Karczewski, M. Pisarek, J.D. Gouveia, J.R.B. Gomes, A. Zielińska-Jurek, J. Phys. Chem. C. 126 (2022) 14859.
[25] X. Ma, Y. Dai, M. Guo, B. Huang, Langmuir 29 (2013) 13647.
[26] M. Lazzeri, A. Vittadini, A. Selloni, Phys. Rev. B - Condens. Matter Mater. Phys. 63 (2001) 1554091.
[27] F. Amano, T. Yasumoto, O.O. Prieto-Mahaney, S. Uchida, T. Shibayama, B. Ohtani, Chem. Commun. (2009) 2311.
[28] J. Li, D. Xu, Chem. Commun. 46 (2010) 2301.
[29] F. Neese, Wiley Interdiscip. Rev.: Comput. Mol. Sci. (2022) 1.
[30] F. Neese, Wiley Interdiscip. Rev.: Comput. Mol. Sci. 2 (2012) 73.
[31] A.D. Becke, J. Chem. Phys. 98 (1993) 5648.
[32] J.C. Zapata, L.K. McKemmish, J. Phys. Chem. A 124 (2020) 7538.
[33] R.G. Parr, R.G. Pearson, J. Am. Chem. Soc. 105 (1983) 7512.
[34] R.G. Parr, L. von Szentpaly, S. Liu, J. Am. Chem. Soc. 121 (1999) 1922.
[35] T. Koopmans, Physica 1 (1934) 104.
[36] D.J. Tozer, F. De Proft, J. Phys. Chem. A 109 (2005) 8923.
[37] X. Wang, L. Sø, R. Su, S. Wendt, P. Hald, A. Mamakhel, C. Yang, Y. Huang, B.B. Iversen, F. Besenbacher, J. Catal. 310 (2014) 100.
[38] A. El Mragui, I. Daou, O. Zegaoui, Catal. Today 321–322 (2019) 41.
[39] X. Guo, H. Yuan, T. Xiao, Y. Wu, Int. J. Biol. Macromol. 131 (2019) 1038.
[40] A.S. Barnard, L.A. Curtiss, Nano Lett. 5 (2005) 1261.
[41] J.J. Murcia, M.C. Hidalgo, J.A. Navío, J. Araña, J.M. Doña-Rodríguez, Appl. Catal. B: Environ. 179 (2015) 305.
[42] Q. Xiang, K. Lv, J. Yu, Appl. Catal. B: Environ. 96 (2010) 557.
[43] M. Maisano, M.V. Dozzi, M. Coduri, L. Artiglia, G. Granozzi, E. Selli, ACS Appl. Mater. Interfaces 8 (2016) 9745.
[44] L. Mino, F. Pellegrino, S. Rades, J. Radnik, V.D. Hodoroaba, G. Spoto, V. Maurino, G. Martra, ACS Appl. Nano Mater. 1 (2018) 5355.
[45] J. Zhang, Y. Nosaka, Appl. Catal. B: Environ. 166–167 (2015) 32.
[46] H. Gong, W. Chu, Y. Huang, L. Xu, M. Chen, M. Yan, Environ. Pollut. 276 (2021) 116691.
[47] J.C.C. Da Silva, J.A.R. Teodoro, R.J.D.C.F. Afonso, S.F. Aquino, R. Augusti, J. Mass Spectrom. 49 (2014) 145.
[48] K.H. Hama Aziz, H. Miessner, S. Mueller, D. Kalass, D. Moeller, I. Khorshid, M.A.M. Rashid, Chem. Eng. J. 313 (2017) 1033.
[49] N. Flores-Holguín, J. Frau, D. Glossman-Mitnik, Molecules (2019) 24.
[50] T. Hathway, W.S. Jenks, J. Photochem. Photobiol. A: Chem. 200 (2008) 216.
[51] S. Moradi, A.A. Isari, F. Hayati, R. Rezaei Kalantary, B. Kakavandi, Chem. Eng. J. 414 (2021) 128618.
[52] C. Minero, G. Mariella, V. Maurino, D. Vione, E. Pelizzetti, Langmuir 16 (2000) 8964.
[53] A.G. Agrios, P. Pichat, J. Photochem. Photobiol. A: Chem. 180 (2006) 130.
[54] K. Lv, X. Guo, X. Wu, Q. Li, W. Ho, M. Li, H. Ye, D. Du, Appl. Catal. B: Environ. 199 (2016) 405.
[55] Y. Sun, J.J. Pignatello, Environ. Sci. Technol. 29 (1995) 2065.
[56] C.S.A. Antunes, M. Bietti, M. Salamone, N. Scione, J. Photochem. Photobiol. A: Chem. 163 (2004) 453.
[57] J.Y. Hwang, G. hee Moon, B. Kim, T. Tachikawa, T. Majima, S. Hong, K. Cho, W. Kim, W. Choi, Appl. Catal. B: Environ. 286 (2021) 119905.
[58] S. Valencia, F. Cataño, L. Rios, G. Restrepo, J. Marín, Appl. Catal. B: Environ. 104 (2011) 300.
[59] F. Amano, K. Nogami, M. Tanaka, B. Ohtani, Langmuir 26 (2010) 7174.